Perturbative approach to the quantum phase transition in the Dicke-Ising chain

Bachelorarbeit aus der Physik

Vorgelegt von
Jonas Leibig

October 4, 2023

Institut für Theoretische Physik I
Friedrich-Alexander-Universität Erlangen-Nürnberg

Betreuer: Prof. Dr. Kai Phillip Schmidt

Abstract

In this thesis, exact high-order series for the ground-state energy and the magnetization are calculated for the Dicke-Ising chain after a displacement transformation and a mean-field decoupling up to order 20 perturbatively in the strong-coupling limit. After that, the limiting cases of the model, which are the Dicke chain and the quantized transverse-field Ising chain without a longitudinal field, are analyzed for ferromagnetic Ising interactions to verify the calculated series. Both cases display different types of quantum phase transitions: the Dicke chain has a second-order transition, while the quantized transverse-field Ising chain without a longitudinal field has a first-order transition. The model has for ferromagnetic interactions a second-order phase transition up to $J = 0.5h$ when approaching from the Dicke limit. In the opposite limit, it becomes evident that the phase transition is of first-order until $J = 2h$. In the region between $J = 0.5h$ and $J = 2h$, it is challenging to definitively classify the order of the phase transition. Furthermore, for antiferromagnetic Ising interactions, our findings match very well with data from quantum Monte Carlo simulations.

Contents

1. Introduction

Quantum mechanics, which originated from Max Planck's groundbreaking quantum hypothesis in 1900, rapidly evolved into one of the most important and far-reaching fields within modern physics. Initially, the quest to understand the behavior of light within the framework of quantum mechanics faced significant challenges. While Erwin Schrödinger's equation provided a powerful tool for explaining non-relativistic quantum phenomena, the treatment of light still remained semi-classical in nature. The turning point came when Paul Dirac started the development of a comprehensive quantum field theory for electrodynamics. This fully describes the complex interplay between light and matter while obeying the principles of quantum mechanics and special relativity. This marked a significant leap forward in our understanding of the quantum nature of electromagnetic interactions. Within the realm of quantum optics, the Dicke model [1] emerged as a fundamental framework. This model treats light as a single quantum mode and matter as a two-level quantum system, providing essential insights into the interaction between these components. To validate and explore the Dicke model's predictions, researchers turned to the field of cavity quantum electrodynamics, where atoms and light are confined within a reflective cavity, enabling controlled experiments and observations.

In this thesis, the Dicke model with a nearest-neighbor Ising interaction is investigated motivated by the work of [2, 3]. This is put into practice by spin-$\frac{1}{2}$ particles on a chain in the thermodynamic limit coupled to light. In [2], a classical mean-field approach to the model was presented. They proposed that all occurring quantum phase transitions in the model with antiferromagnetic interactions are of second-order. However, this assertion was disproved by [3], who analyzed the limiting case with no longitudinal field. This led to further investigations into the quantum phase transitions in the model, particularly in the unexplored ferromagnetic case. The introduction to the model includes simplifications such as a displacement transformation and a mean-field decoupling, along with methods to calculate the ground-state energy and magnetization of the model in section 2. Following that, we introduce extrapolation techniques aimed at enhancing the series convergence and to classify the critical behavior at the quantum phase transition in section 3. In section 4, the analysis of quantum phase transitions in the ferromagnetic case is discussed, and the point at which the transition changes from first to second-order is determined. Finally, in section 5, a brief investigation into the antiferromagnetic case is presented to compare the calculated observables with data from quantum Monte Carlo simulations (QMC) provided by Anja Langheld [1].

[1] Anja Langheld, Institut für Theoretische Physik I, Universität Erlangen-Nürnberg, anja.langheld@fau.de

2. Model

In the following section, the Dicke-Ising chain (DIC) is introduced. Furthermore, the techniques to calcuate the ground-state energy and the magnetization of the system are presented.

2.1. Hamiltonian

The DIC is the combination of the well-known Dicke model [1] with an additional nearest-neigbor Ising interaction [4]. The two Hamiltonians are defined in the same way as in [3] and are given by

$$\hat{\mathcal{H}}_{\text{Dicke}} = \omega_0 \hat{S}_z + \frac{g}{\sqrt{N}} \left(\hat{a}^\dagger + \hat{a}\right) \hat{S}_x + \omega_c \hat{a}^\dagger \hat{a}, \tag{1}$$

$$\hat{\mathcal{H}}_{\text{Ising}} = -J \sum_{\langle i,j \rangle} \sigma_i^z \sigma_j^z, \tag{2}$$

where J specifies the strength of the nearest-neighbor interaction. A positive (negative) sign of J indicates a (anti-) ferromagnetic Ising interaction. $\hat{S}_i = \sum_k \frac{\sigma_k^i}{2}, i \in \{x, y, z\}$ denotes the collective spin operators, written in natural units as used in the whole thesis, with the Pauli matrices σ^i. $\hat{a}$ and $\hat{a}^\dagger$ are the bosonic annihilation and creation operators, which satisfy the commutator relation $\left[\hat{a}, \hat{a}^\dagger\right] = 1$. These operators, respectively, can destroy and create a light mode at frequency ω_c. ω_0 gives the strength of the longitudinal field in z direction. The parameter g is the photon-spin coupling and tunes the collective interaction of all spins with the bosonic light modes. The Hamiltonian of the DIC as the sum of the two Hamiltonians reads

$$\hat{\mathcal{H}}_{\text{DIC}} = -J \sum_{\langle i,j \rangle} \sigma_i^z \sigma_j^z + \omega_0 \hat{S}_z + \frac{g}{\sqrt{N}} \left(\hat{a}^\dagger + \hat{a}\right) \hat{S}_x + \omega_c \hat{a}^\dagger \hat{a}. \tag{3}$$

2.2. Displacement transformation

In order to make the calculations easier, the Hamiltonian is transformed as in [3] with a displacement operator $\hat{D}(\alpha) \coloneqq \exp\left[\alpha \hat{S}_x \left(\hat{a}^\dagger - \hat{a}\right)\right]$, where $\alpha \coloneqq \frac{g}{\omega_c \sqrt{N}}$. This unitary operator has the ability to displace a vacuum state into a coherent state in the photon subspace $\hat{S}_x |\alpha\rangle = \hat{D}(\alpha) |0\rangle$ with an amplitude depending on the value of the $\hat{S}_x$ operator, which lives in the Hilbert space of the spins [3]. A coherent state is defined as the eigenstate of the annihilation operator $\hat{a}$ [5]. For the case $\omega_0 = 0$, the displacement transformation makes the problem trivial because it diagonalizes the Hamiltonian. The effect of the displacement transformation on the ladder operators can be easily calculated with the Baker-Campbell-Hausdorff-Formula

$$e^{\hat{A}} \hat{B} e^{-\hat{A}} = \sum_{m=0}^{\infty} \frac{1}{m!} \left[\hat{A}, \hat{B}\right]_m, \tag{4}$$

$$\text{with } \left[\hat{A}, \hat{B}\right]_m = \left[A, \left[\hat{A}, \hat{B}\right]_{m-1}\right] \text{ and } \left[\hat{A}, \hat{B}\right]_0 = \hat{B}. \tag{5}$$

The result is

$$\hat{D}^\dagger \hat{a} \hat{D} = \hat{a} + \alpha \hat{S}_x, \tag{6}$$

$$\hat{D}^\dagger \hat{a}^\dagger \hat{D} = \hat{a}^\dagger + \alpha \hat{S}_x. \tag{7}$$

This means, the displacement transformation shifts the ladder operators by $\alpha \hat{S}_x$. After that, the only missing part to transform the whole Hamiltonian is the action of the displacement operator on the Pauli z matrix and the product of two Pauli z matrices. This calculation is straightforward using the Baker-Campbell-Hausdorff-Formula and the two commutation relations

$$\left[\frac{\sum_i \sigma_i^x}{2}, \sum_j \sigma_j^z\right]_m = \begin{cases} -i\sigma_i^y \, \delta_{ij}, & \text{m odd} \\ \sigma_i^z \, \delta_{ij}, & \text{m even} \end{cases} \tag{8}$$

and

$$\left[\frac{\sum_i \sigma_i^x}{2}, \sum_j \sigma_j^z \sigma_{j+1}^z\right]_m = \begin{cases} -2^m i \, (yz + zy), & \text{m odd} \\ 2^m \, (zz - yy) & \text{m even} \end{cases}. \tag{9}$$

Here we introduced the notation $\alpha\beta \coloneqq \sum_i \sigma_i^\alpha \sigma_{i+1}^\beta$ and in the following $\hat{r} := \alpha \left(\hat{a}^\dagger - \hat{a}\right)$ is used. With the help of the above derived identities, the Hamiltonian can be displaced and reads

$$\begin{aligned} \hat{\mathcal{H}} = \hat{D}\hat{\mathcal{H}}_{\mathrm{DIC}}\hat{D}^\dagger = &- J \left[zz + \frac{1}{2}\,(zz - yy)\,(\cosh 2\hat{r} - \mathbb{1}) - \frac{i}{2}\,(yz + zy)\sinh 2\hat{r}\right] \\ &+ \omega_0 \left[\hat{S}_z \cosh \hat{r} - i\hat{S}_y \sinh \hat{r}\right] + \omega_c \left[\hat{a}^\dagger \hat{a} - \alpha^2 \hat{S}_x^2\right]. \end{aligned} \tag{10}$$

In the regime of interest, we know that α is small, because we are in the thermodynamic limit. Therefore, we can write the Hamiltonian as

$$\hat{\mathcal{H}} = \omega_c \hat{a}^\dagger \hat{a} - \frac{g^2}{\omega_c N} \hat{S}_x^2 + \omega_0 \hat{S}_z - J \sum_{\langle i,j \rangle} \sigma_i^z \sigma_j^z. \tag{11}$$

2.3. Mean-field decoupling

The last step applied to the model is a mean-field decoupling on $\hat{S}_x^2$. By this approach, the model transforms into a non-interacting spin system that interacts with a mean field. Therefore, light and matter can be considered separately. This gives a simpler Hamiltonian that can be investigated. Notably, in dimensions four and above, the mean-field theory gives the correct critical behavior of the classical Ising model [6].

The decoupling can be performed by expressing $\hat{S}_x$ by its mean value plus its fluctuation

$$\hat{S}_x = \langle \hat{S}_x \rangle + \delta \hat{S}_x. \tag{12}$$

By looking at the square of $\hat{S}_x$, the term $\delta\hat{S}_x^2$ is neglected

$$\begin{aligned}\hat{S}_x^2 &= \langle\hat{S}_x\rangle^2 + 2\langle\hat{S}_x\rangle\delta\hat{S}_x + \delta\hat{S}_x^2 \approx \langle\hat{S}_x\rangle^2 + 2\langle\hat{S}_x\rangle\delta\hat{S}_x \\ &= \langle\hat{S}_x\rangle(\langle\hat{S}_x\rangle + 2\delta\hat{S}_x) \overset{(12)}{=} \langle\hat{S}_x\rangle(\langle\hat{S}_x\rangle + 2\hat{S}_x - 2\langle\hat{S}_x\rangle) \\ &= \langle\hat{S}_x\rangle(2\hat{S}_x - \langle\hat{S}_x\rangle) = -\langle\hat{S}_x\rangle^2 + 2\langle\hat{S}_x\rangle\hat{S}_x\end{aligned}$$

The mean value of $\hat{S}_x$ is defined as the Magnetization $M_x \equiv \langle\hat{S}_x\rangle$

$$\hat{S}_x^2 \approx -M_x^2 + 2M_x\hat{S}_x. \tag{13}$$

After this, the decoupling is done and the Hamiltonian reads

$$\hat{\mathcal{H}} = \frac{g^2N}{\omega_c}m_x^2 + \omega_c\hat{a}^\dagger\hat{a} - \frac{g^2}{\omega_c}m_x\sum_i\sigma_i^x + \frac{\omega_0}{2}\sum_i\sigma_i^z - J\sum_{\langle i,j\rangle}\sigma_i^z\sigma_j^z, \tag{14}$$

with the magnetization per site $m_x = \frac{M_x}{N}$.

2.4. Effective Hamiltonian

For convenience, we calculate the high order series expansions in a different basis:

$$\hat{\mathcal{H}}_{\text{eff}} = -2m_z\sum_i\sigma_i^z + J\sum_{\langle i,j\rangle}\sigma_i^x\sigma_j^x + h\sum_i\sigma_i^x. \tag{15}$$

The reason for this is, that the calculation are easier on the effective Hamiltonian. This Hamiltonian can be one to one mapped on the previous Hamiltonian for the observables we want to investigate like the ground-state energy and the magnetization. The change from the Pauli z to the Pauli x matrix and vice versa can be performed by a change of basis, which can be done by rotating the system 90 degrees around the y-axis.

2.5. Ground-state energy

The analyzed model is not integrable, which means it is not possible to find an exact solution for the eigenstates. A common way to treat such problems is to calculate the energy perturbatively. This is done by splitting the Hamiltonian in an unperturbated exactly solveable Hamiltonian $\hat{\mathcal{H}}_0$ and a perturbation V, which is tuned by a small parameter λ,

$$\hat{\mathcal{H}} = \hat{\mathcal{H}}_0 + \lambda V,\ \lambda \in [0,1]. \tag{16}$$

For $\lambda = 0$ we have the unperturbed Hamiltonian and for $\lambda = 1$ the fully perturbed Hamiltonian. After that the goal is to approximate the energy as a power series in λ

$$E = \sum_{i=0}^{\infty}\lambda^i E_i. \tag{17}$$

Here E_0 is the energy of the unperturbed Hamiltonian and E_i is the energy correction of i-th order. It is also possible to expand the eigenstate to the eigenvalue E, but here it is sufficient to consider the ground-state energy without its eigentates. This procedure for quantum mechanics was first done by Schrödinger in 1926 [7]. An easy way to calculate the energy corrections is to use the coefficients derived by Löwdin [8], who tackled the problem with an projection operator formalism. By using these, one can achieve corrections up to high order using a computer.

In the model investigated in this thesis, the unperturbed Hamiltonian and the perturbation read

$$\hat{\mathcal{H}}_0 = -2m_z \sum_i \sigma_i^z, \tag{18}$$

$$V = J \sum_{\langle i,j \rangle} \sigma_i^x \sigma_j^x + h \sum_i \sigma_i^x. \tag{19}$$

The unique ground state of $\hat{\mathcal{H}}_0$ is $|0\rangle = |\uparrow ... \uparrow\rangle := |\Uparrow\rangle$ with eigenvalue $E_0^0 = -2m_z N$. After transferring this into the language of Löwdins projection operator formalism, we have

$$\begin{aligned} &P = 1 - Q = |0\rangle \langle 0| \text{ the projector onto the ground state,} \\ &V = J \sum_{\langle i,j \rangle} \sigma_i^x \sigma_j^x + h \sum_i \sigma_i^x \text{ the perturbation and} \\ &S = Q \frac{1}{E_0^0 - \hat{\mathcal{H}}_0} Q \text{ the resolvent.} \end{aligned} \tag{20}$$

The first energy correction given by Löwdin

$$E_0^1 = \langle P|V|P\rangle = 0 \tag{21}$$

vanishes for our model. The corrections up to order four were calculated by hand with the help of the linked-cluster expansion introduced by Marland in 1981 [9]. Higher orders were calculated with the help of a computer.

2.6. Magnetization

Another important property of the system is the magnetization, because it is the magnetic order parameter in the ferromagnetic case, which is analyzed. The magnetization is defined as the expectation value of the collective spin operator in the ground state

$$M_\alpha = \langle 0| \hat{S}_\alpha |0\rangle = \left\langle 0 \middle| \frac{\sum_i \sigma_i^\alpha}{2} \middle| 0 \right\rangle. \tag{22}$$

Of particular interest is the z magnetization because it is in our unperturbed Hamiltonian. So it is necessary to calculate the z magnetization to get an actual value for our ground state-energy. By looking at Equation 22, one sees that it is also required to know all the corrections to the ground state. However, by using the Hellmann-Feynman theorem [10] it is possible to avoid these corrections. The theorem states, applied

to our problem,

$$\frac{\mathrm{d}E_0(m_z)}{\mathrm{d}m_z} = \left\langle 0 \left| \frac{\mathrm{d}H(m_z)}{\mathrm{d}m_z} \right| 0 \right\rangle = -2 \left\langle 0 \left| \sum_i \sigma_i^z \right| 0 \right\rangle = -4 \left\langle 0 \left| \hat{S}_z \right| 0 \right\rangle . \tag{23}$$

$$\implies m_z = -\frac{1}{4} \frac{\mathrm{d}}{\mathrm{d}m_z} \frac{E_0}{N} . \tag{24}$$

So it is possible to calculate the z magnetization by taking the derivative of the ground-state energy up to some constant. Thereby, we get the magnetization to the same order as the ground-state energy.

3. Approach

3.1. Perturbative solution of the self-consistent mean-field equation

The series of the ground-state energy of the effective Hamiltonian Equation 15 was determined perturbatively. However, in the series the magnetization m_z is still present because it is in the prefactor of the term $\sum_i \sigma_i^z$. So, for example, the energy up to second-order is

$$\frac{E_0(J,h,m_z)}{N} = -2m_z - \left(\frac{J^2}{8m_z} + \frac{h^2}{4m_z}\right) + \mathcal{O}(3). \tag{25}$$

As a result of this, it is necessary to determine the magnetization as a function of J and h in order to obtain the energy as a function of J and h. This can be done by using Equation 24. So we get for the magnetization up to second-order

$$m_z(J,h,m_z) = \frac{1}{2} - \frac{J^2}{32m_z^2} - \frac{h^2}{16m_z^2} \tag{26}$$

This type of equation is called a self-consistent equation, because the function m_z depends on m_z itself. It is possible to solve this equation for m_z perturbatively. Therefore we need to make an ansatz for m_z, put it in Equation 26 and Taylor expand the expression in J and h to the same order as the magnetization. So for our example we make the ansatz

$$m_z(J,h) = \frac{1}{2} + aJ^2 + bh^2 \tag{27}$$

because $\frac{1}{2}$ is the magnetization of our unperturbed Hamiltonian and a and b are constants that get determined in the following step. If we put Equation 27 in Equation 26 and Taylor expand it to the second-order, we get

$$m_z(J,h) = \frac{1}{2} - \frac{J^2}{8} - \frac{h^2}{4}. \tag{28}$$

After this, the procedure can be repeated order by order. For the next order, three, one would have to use an ansatz of the form Equation 28 plus the variation of the third order term

$$m_z(J,h) = \frac{1}{2} - \frac{J^2}{8} - \frac{h^2}{4} + cJh^2, \tag{29}$$

plug it into the self-consistent equation and Taylor expand it. This process is done to the same order as the ground-state energy was determined as a high-order series expansion. For our case it was up to order 20. In subsection A.1 the full series of the magnetization is shown.

3.2. Ground-state energy

The ground-state energy of our Hamiltonian after the mean-field decoupling in Equation 14 can be calculated with the help of the ground-state energy of the effective Hamiltonian in Equation 15. This can be easily

shown by putting the two Hamiltonians side by side.

$$\hat{\mathcal{H}}_{eff} = -2m_z \sum_i \sigma_i^z + J \sum_{\langle i,j \rangle} \sigma_i^x \sigma_j^x + h \sum_i \sigma_i^x$$

$$\hat{\mathcal{H}} = \frac{g^2 N}{\omega_c} m_x^2 + \omega_c \hat{a}^\dagger \hat{a} - \frac{g^2}{\omega_c} m_x \sum_i \sigma_i^x - J \sum_{\langle i,j \rangle} \sigma_i^z \sigma_j^z + \frac{\omega_0}{2} \sum_i \sigma_i^z$$

The colored terms can be mapped onto each other by changing the constants in front of the sums in the calculations and transform the basis to change the Pauli z to a Pauli x matrix and vice versa like in subsection 2.4. The extra term $\omega_c \hat{a}^\dagger \hat{a}$ is neglected, because the lowest energy is achieved when no light mode is present in the system. The part with m_x^2 can be calculated because the self-consistent equation for the magnetization is solved in subsection 2.6. For Example, for the special case $\frac{g^2}{\omega_c} = 2$, the ground-state energy per site is

$$\frac{E_0}{N} = e_0 = 2 \cdot m^2 + E_{\hat{\mathcal{H}}_{eff}}. \tag{30}$$

The energy of the effective Hamiltonian can be calculated by inserting the magnetization in the series obtained with the computer doing a Taylor expansion in J and h up to the wanted order. For the second-order we get the result

$$e_0 = -\frac{1}{2} - \frac{h^2}{2} - \frac{J^2}{4}. \tag{31}$$

The higher orders are listed in subsection A.2.

3.3. Extrapolation

It is possible to improve the convergence of the calculated series by using extrapolation techniques. This approach enables the analysis of the energy and the magnetization for larger perturbation parameters (J and h) compared to using the bare series. The first technique is the Padé approximation [11], which is the best approximation of a function by a rational function. For a known power series $f(x) = \sum_{k=0}^{r} c_k x^k$ up to order r, the Padè approximation is defined as in [12] as

$$P[n,m]_f := \frac{P_n(x)}{Q_m(x)} = \frac{\sum_{k=0}^{n} p_k x^k}{\sum_{k=0}^{m} q_k x^k}. \tag{32}$$

To calculate the the coefficients p_k and q_k, we use that the Padé series has to be the same as the power series $f(x)$ up to order $r = n + m$. This gives you the following set of linear equations

$$\frac{\mathrm{d}^k}{\mathrm{d}x^k} P[n,m]_f \bigg|_{x=0} = \frac{\mathrm{d}^k}{\mathrm{d}x^k} f(x) \bigg|_{x=0}, \tag{33}$$
$$k \in \{0, 1, ..., r\}$$

which define the parameters p_k and q_k uniquely. Our power series is defined by its order r but there are many Padé extrapolants that satisfy $r = n + m$. It is also possible to approximate the power series of a pair (n, m) which are smaller than r. So there are many Padé approximations for a single power series, which can all be used to analyze the power series. However, not every Padé approximation is useful. One has to compare the different extrapolants to see if they look the same. This way you make sure that your Padé

converge better than the normal power series. Furthermore, the different combinations of m and n for a single r have different poles, which can be physical or not. To extract the physical ones, one can use the technique presented in [13].

Another methodis the dlog-Padé extrapolation, which is the Padé approximation applied to the derivative of the logarithm for a given power series. This reads

$$P[n,m]_{\frac{\mathrm{d}}{\mathrm{d}x}\ln f(x)} = \frac{P_n(x)}{Q_m(x)} \tag{34}$$

with $n+m = r-1$ because of the derivative. To go back to our proper power series, we have to apply the exponential function and integrate

$$\mathrm{d}P[n,m]_f \coloneqq \exp\left(\int_0^x \mathrm{d}t \frac{P_n(t)}{Q_m(t)}\right). \tag{35}$$

The advantage of the dlog-Padé is that it is useful to describe the behavior of a function at a pole, which is a root of the denominator of the dlog-Padé. One can approximate a singular function near a critical point x_c as

$$f(x) = \left(1 - \frac{x}{x_c}\right)^{-\beta}. \tag{36}$$

The residual of the dlog-Padé at the critical point specifies the critical exponent β and is given by

$$\beta = \left.\frac{P_n(x)}{\frac{\mathrm{d}}{\mathrm{d}x}Q_m(x)}\right|_{x=x_c}. \tag{37}$$

This is applied to the magnetization to investigate its behavior near the critical point, where it can be approximated as

$$m(\lambda) = |\lambda - \lambda_c|^{\beta}. \tag{38}$$

The poles of the dlog-Padé can be again filtered with the same method as for the normal Padé extrapolation. It is common to classify Padé/dlog-Padé-extrapolants into families. One family is defined by a constant $\Delta = n-m$, with $r \geq n+m \,/\, r-1 \geq n+m$. Each member has a different maximal order $n+m$. By looking at increasing $n+m$ in a family the members should converge toward a similar behavior. After that, one can compare the highest members of different families to analyze the quality of a series extrapolation and to filter out not significant Padés.

4. Results: ferromagnetic Ising interactions

The goal of the thesis is to analyze the quantum phase transition in the Dicke-Ising chain. The main focus lies on ferromagnetic Ising interactions in the chain. In this case, two phases are expected. In the investigated limit, the phase is the superradiant phase with high light-matter interactions, while in the weak-coupling limit, the phase is a magnetically ordered phase with no light-matter interactions. The series of the ground-state energy and the magnetization were calculated and can be plotted to visualize the quantum phase transition. This is done for fixed values of $\frac{J}{h}$ to simplify the problem to only one parameter. The point of the quantum phase transition is found at the intersection of the ground-state energy of the Hamiltonian Equation 14 and the ground-state energy of the weak-coupling limit, which is just a straight line in the thermodynamic limit because the ground state energy of this magnetically ordered phase does not depend on the light-matter interactions. The calculated series in the limiting cases are correct because these cases have an analytical solution that can be Taylor expanded to the given order. The effective Hamiltonian for $J = 0$ can be easily diagonalized and for $h = 0$ the solution was given in [14].

4.1. Limiting cases

At first, the two limiting cases were analyzed. For the case $\omega_0 = 0$, the model simplifies to the quantized transverse-field Ising chain without a longitudinal field (QFTIM)

$$\hat{\mathcal{H}}_{\mathrm{QFTIM}} = -J \sum_{\langle i,j \rangle} \sigma_i^z \sigma_j^z + \frac{g}{\sqrt{N}} \left(\hat{a}^\dagger + \hat{a} \right) \hat{S}_x + \omega_c \hat{a}^\dagger \hat{a}. \tag{39}$$

For this model a quantum phase transition of first order is expected.

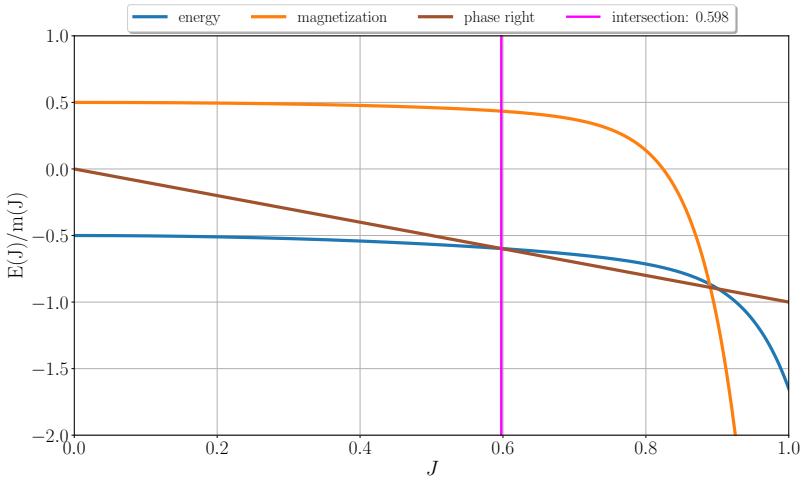

Figure 1: Bare series of the ground-state energy per site and magnetization for the case $\omega_0 = 0$. This corresponds to the quantized transverse-field Ising chain without a longitudinal field. A first-order quantum phase transition takes place at $J \approx 0.598$.

Figure 1 shows the behavior of the series of the ground-state energy and the magnetization for the only J case. The plot verifies the expected behavior. The intersection of the two energies occurs at $J = 0.598$. This value was also calculated by [3]. Furthermore, the order of the quantum phase transition is first-order because the magnetization does not drop to zero at the point of intersection.

The other limiting case is for $J = 0$ the pure Dicke chain

$$\hat{\mathcal{H}}_{\text{Dicke}} = \omega_0 \hat{S}_z + \frac{g}{\sqrt{N}} \left(\hat{a}^\dagger + \hat{a}\right) \hat{S}_x + \omega_c \hat{a}^\dagger \hat{a}. \tag{40}$$

The quantum phase transition of the Dicke model is of second-order and has the mean field critical exponent of $\beta = \frac{1}{2}$ for the magnetization.

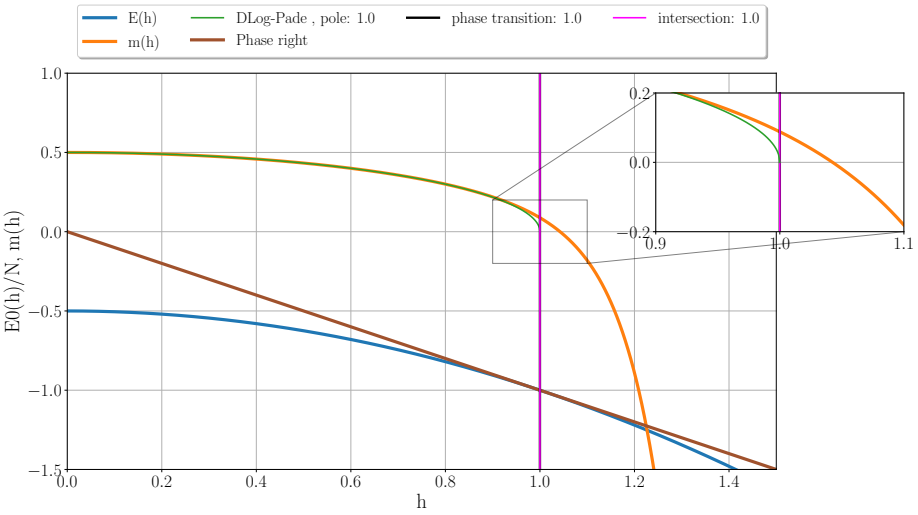

Figure 2: Bare series of the ground-state energy and magnetization for the $J = 0$ case. This corresponds to the Dicke chain. A quantum phase transition of second-order occurs at $h_{\text{crit}} = 1$ with a critical exponent $\beta = \frac{1}{2}$.

In Figure 2 the ground-state energy and magnetization are plotted with the series obtained from the perturbative approach. The two energies meet exactly at $h_{\text{crit}} = 1$. The magnetization drops to zero at this point and the critical point can be analyzed with the help of dlog-Padés. For this case the dlog-Padé is exact and is

$$P[n,m]_{\frac{\mathrm{d}}{\mathrm{d}h} \ln m(h)} = \frac{-h}{1-h^2} \tag{41}$$

in all orders. The poles of this function are at $h_{\text{crit}} = \pm 1$. This fits with the intersection of the two energy. The critical exponent, as defined in Equation 37, is determined by the residual of the function at the critical point

$$\beta = \left.\frac{P_n(h)}{\frac{\mathrm{d}}{\mathrm{d}h} Q_m(h)}\right|_{h=h_c} = \left.\frac{-h}{-2h^2}\right|_{h=1} = \frac{1}{2}. \tag{42}$$

so, the calculated series gives the expected mean-field criticality.

The two limiting cases showed that the perturbative approach to calculate the series worked well in the two

limits and now values inbetween can be analyzed. The goal is to determine the phase transition line and to locate when the system changes from first to second order.

4.2. Small $\frac{h}{J}$

By gradually increasing the value of h, it is possible to investigate the influence of the longitudinal field on both the ground-state energy and the magnetization.

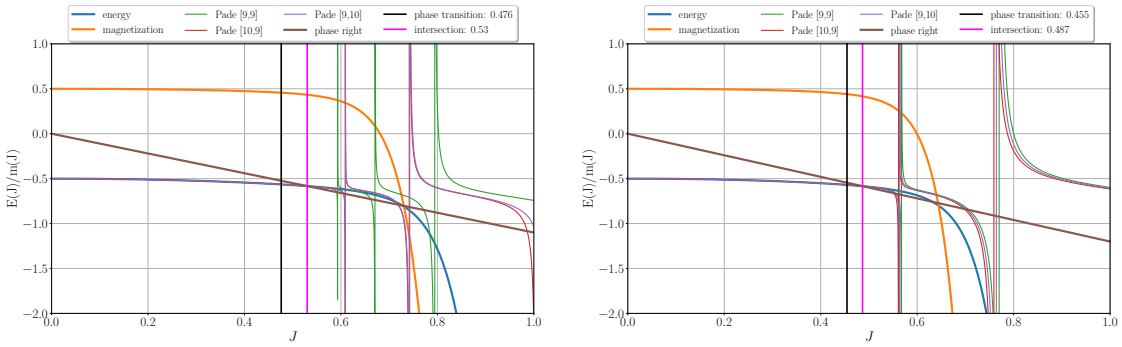

(a) $J = 10h$ (b) $J = 5h$

Figure 3: Ground-state energy and magnetization for the case $J = 10h$ and $J = 5h$. The quantum phase transition happening in the two plots are of first-order because the magnetization does not have a pole at the point of the expected transition.

Figure 3 shows this for the ratios $J = 10h$ and $J = 5h$. In the plots is in orange the magnetization, in blue the ground-state energy and in brown the energy of the phase from the right. There are also some Padés plotted for the energy. These have a nice behavior and only have poles after the quantum phase transition, where the series becomes unphysical due to the invalidity of our assumptions in this region. The vertical line in magenta defines the intersection of the two energies and the black line the point of the expected quantum phase transition of second-order. The expected value for the second-order quantum phase transition can be calculate via

$$J_{\text{crit}} = \frac{1}{2 + \frac{h}{J}} \quad \text{or} \quad h_{\text{crit}} = \frac{1}{1 + 2\frac{J}{h}} \tag{43}$$

depending on the varied parameter. Comparing the difference of the two vertical lines one can notice that for $J = 10h$ the value (≈ 0.054) is larger than for $J = 5h$ (≈ 0.032). So the the two lines are getting closer when increasing h. This indicates that the quantum phase transition occurring in the two plots remains a first-order transition, as it does not coincide with the expected critical point, similar to the case $h = 0$. Additionally, the magnetization does not decrease to zero, as one would expect for a second-order quantum phase transition. Furthermore, the energies exhibit a sharp intersection, a characteristic of a first-order transition. In contrast, a second-order transition would typically involve only a mere touching of the energy curves. So, we need to increase h to larger values to observe a change in the order of the quantum phase transition.

The next two investigated ratios are $J = 2h$ and $J = h$.

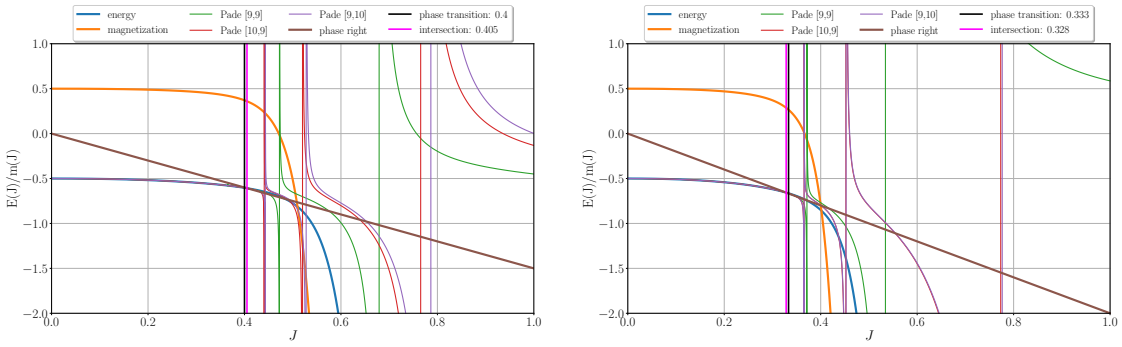

(a) $J = 2h$ (b) $J = h$

Figure 4: Ground-state energy and magnetization for the case $J = 2h$ and $J = 1h$. The quantum phase transition happening in the two plots seem to change between these two ratios of J and h because the intersection of the energies happens for $J = h$ before the calculated value.

In Figure 4 are the same parameters as in Figure 3 plotted for these two ratios. The energy and magnetization convergence nicely to the intersection and to the expected value of the quantum phase transition. For $J = 2h$ the expected value is lower than the actual intersection, but for $J = h$, this changes. This suggests a possible change in the order of the quantum phase transition. To provide a more precise statement, a closer examination of the magnetization's behavior near the transition is necessary. Before proceeding, we investigate the behavior of the ground-state energy and magnetization from the opposite limit $J = 0$. This way we can localize the transition from first to second order quantum phase transition from both limits.

4.3. Small $\frac{J}{h}$

As mentioned earlier, the limiting case where $J = 0$ corresponds to the Dicke chain. For this we know that a quantum phase transition of second-order with a critical exponent of $\beta = \frac{1}{2}$ occurs. Initially, the cases $J = \frac{h}{10}$ and $J = \frac{h}{5}$ are examined.

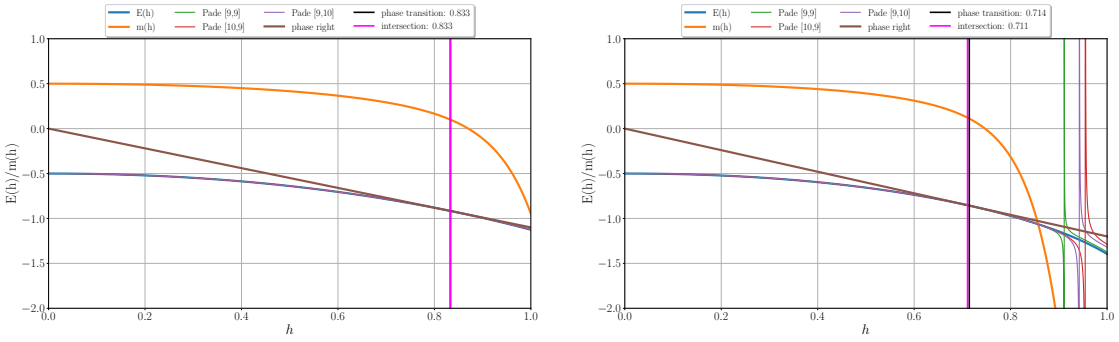

(a) $J = \frac{h}{10}$ (b) $J = \frac{h}{5}$

Figure 5: Ground-state energy and magnetization for the case $J = \frac{h}{10}$ and $J = \frac{h}{5}$. The intersection of the two energies match the expected value very good. The quantum phase transition is of second-order.

Figure 5 supports the assumption that for small J the ground-state energy and the magnetization behave like in the pure Dicke chain. The intersection of the two energies fits the expected value of the quantum phase transition very good. The magnetization almost drops to zero at the intersection. To demonstrate that the quantum phase transition is indeed of the second-order, it is necessary to create dlog-Padés for the magnetization and then examine its behavior at the quantum phase transition.

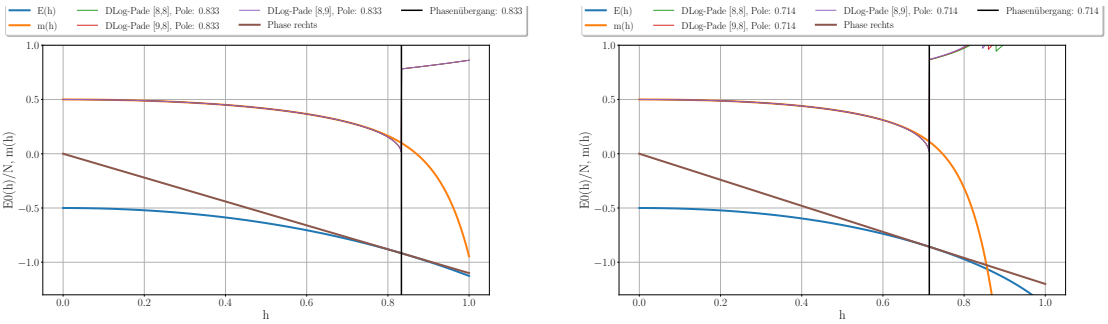

(a) dlog-Padé for $J = \frac{h}{10}$ (b) dlog-Padé for $J = \frac{h}{5}$

Figure 6: Dlog-Padés for $J = \frac{h}{10}$ and $J = \frac{h}{5}$ of the magnetization. These possess a pole precisely at the quantum phase transition, thereby is the transition of second-order.

Figure 6 shows these approximations. In the legend of the plot the position of the pole is also shown. It can be observed that when $J = \frac{h}{10}$ and $J = \frac{h}{5}$, the poles of the magnetization coincide with the energy intersection points, signalizing the point of the quantum phase transition. The analysis of the critical exponent for this quantum phase transition is discussed in the following section. Therefore, when we deviate slightly from the limiting case $J = 0$, the quantum phase transition remains of the same order as the limiting case.

The next two ratios under analysis are $J = \frac{h}{2}$ and $J = h$. The latter has already been studied from the opposite limit.

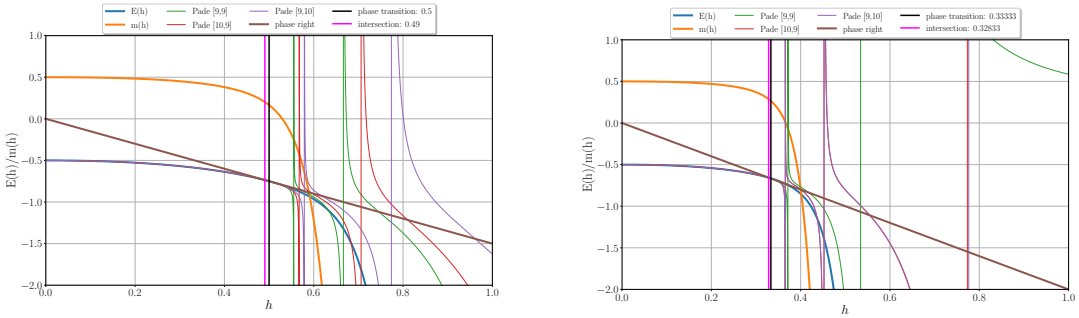

(a) $J = \frac{h}{2}$ (b) $J = h$

Figure 7: Ground-state energy and magnetization for the ratios $J = \frac{h}{2}$ and $J = h$.

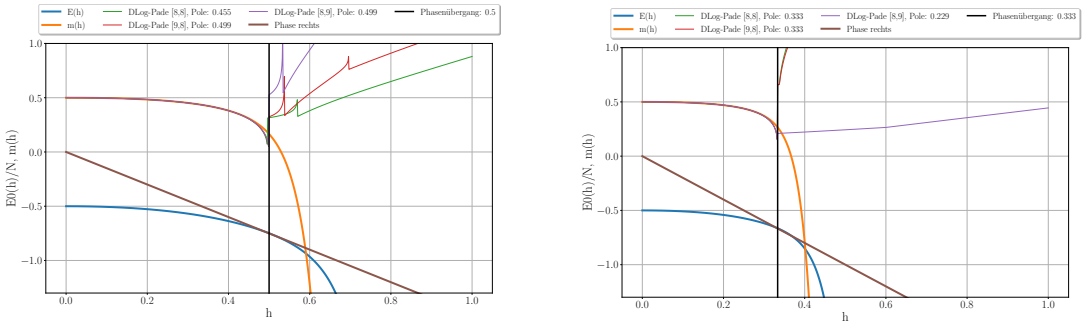

(a) dlog-Padé for $J = \frac{h}{2}$ (b) dlog-Padés for $J = h$

Figure 8: Dlog-Padés of magnetization for the ratios $J = \frac{h}{2}$ and $J = h$. The quantum phase transition still seems to be of second-order but it is not as obvious as in the previous cases.

These two cases still show a behavior of a second-order quantum phase transition. This is visualized in Figure 7. The energies touch at the expected value and the magnetization still drops a bit at the transition. Examining the dlog-Padés of the magnetization in Figure 8 reveals the presence of a pole at the expected value in each case. However, it is worth noting that there is a slight deviation in one dlog-Padé in each plot. A more in-depth analysis involving multiple dlog-Padés is presented in the following section, as previously mentioned. So, it is still necessary to go to higher ratios of $\frac{J}{h}$ to observe the transition from first to second order. That is done by looking at $J = 1.5h$ and $J = 2h$.

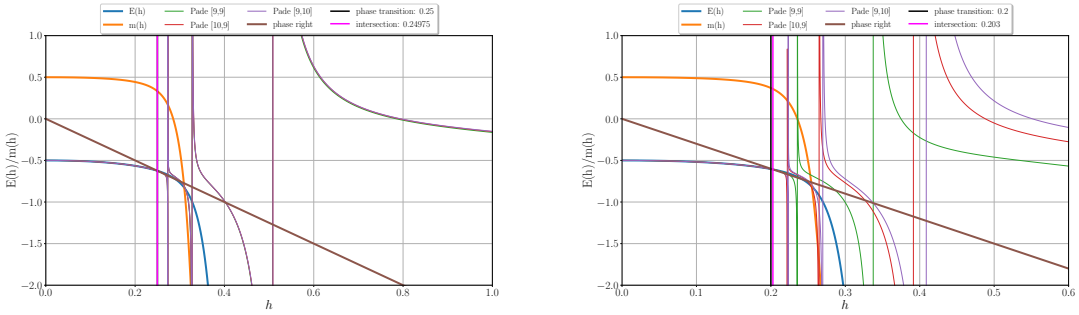

(a) $J = 1.5h$ (b) $J = 2h$

Figure 9: Ground-state energy and magnetization for the ratios $J = 1.5h$ and $J = 2h$.

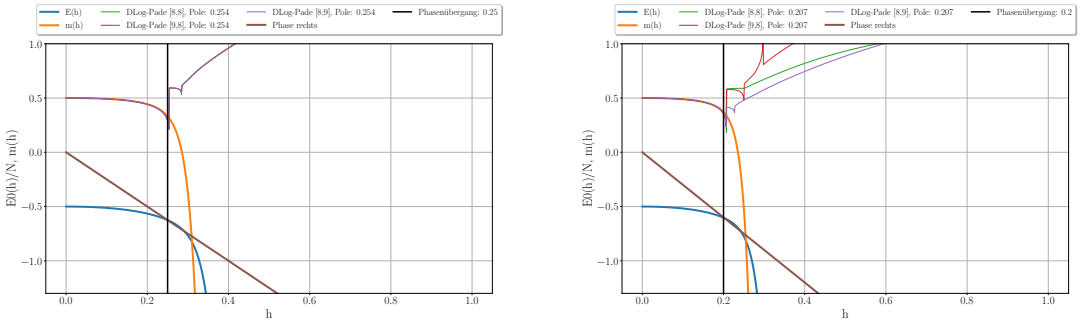

(a) Dlog-Padé for $J = 1.5h$ (b) Dlog-Padé for $J = 2h$

Figure 10: Dlog-Padés of the magnetization for the ratios $J = 1.5h$ and $J = 2h$.

This is visualized in Figure 9. The energies continue to exhibit the expected behavior characteristic of a second-order quantum phase transition. However, when $J = 2h$, the intersection occurs prior to the calculated quantum phase transition point, suggesting the possibility of a first-order transition in this particular case. When examining the dlog-Padés of these two cases in Figure 10, one can still observe poles at the anticipated value, but they begin to shift away from it. When closely examining the various ratios close to the Dicke limit, it becomes evident that we can narrow the potential change in the order of the quantum phase transition within the range of $J = 1.5h$ to approximately $J = 2h$. This is because, in the latter case, the intersection of energies occurs prematurely relative to expectations, and the poles also exhibit a deviation from the anticipated value.

4.4. Examining the shift in the order of the quantum quantum phase transition

In the following, we will examine the location of the change in the order of the quantum phase transition in more detail. This will be accomplished by analyzing the poles of the dlog-Padés of the magnetization and observing the behavior of the critical exponent at the quantum phase transition. To achieve this, we will

compare the dlog-Padés within a family to compare their convergence toward the expected value. At first the case $J = 0.1h$ is presented to see how these quantities should behave at a second-order quantum phase transition. The families $\Delta = \pm 1$ are plotted in the following because for these families many dlog-Padés can be compared. The families $0, \pm 2, \pm 3$ were also calculated but they show a similar behavior as the one shown. For $J = 0.1h$ the members of the family with higher order of n lie at the expected value as shown in Figure 11. The blue points represent the position of the pole and the blue line the expected value of the quantum phase transition calculated with Equation 43. In red is the calculated critical exponent in comparison to the expected Dicke criticality.

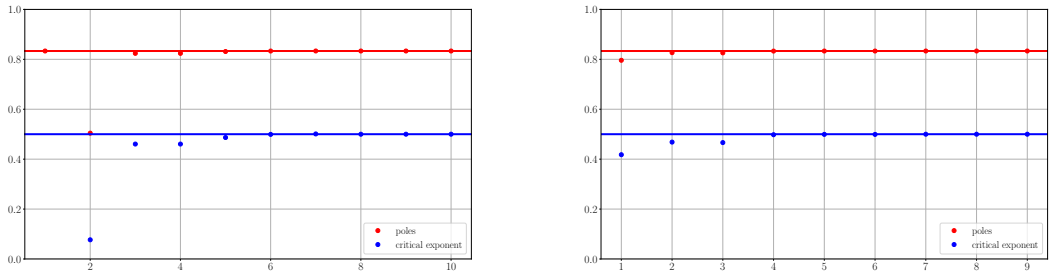

(a) $\Delta = +1$ (b) $\Delta = -1$

Figure 11: Comparison of the critical exponent and the position of poles with their expected values for the ratio $J = 0.1h$ for the families $\Delta = \pm 1$.

Now, the ratio is moved more closely to the range where the change in the order is expected to occur.

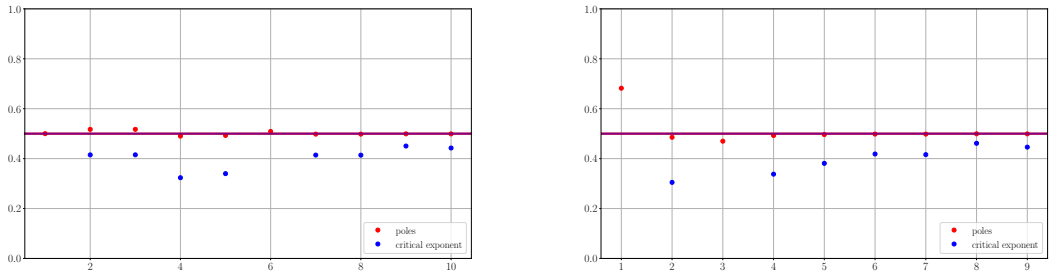

(a) $\Delta = +1$ (b) $\Delta = -1$

Figure 12: Comparison of the critical exponent and the position of poles with their expected values for the ratio $J = 0.5h$ for the families $\Delta = \pm 1$.

For $J = 0.5h$ in Figure 12 the poles still converge against the expected value but the critical exponent has some variability and does not convergence towards 0.5. That behavior cannot be easily explained, but it might be explained by the next ratio $J = h$.

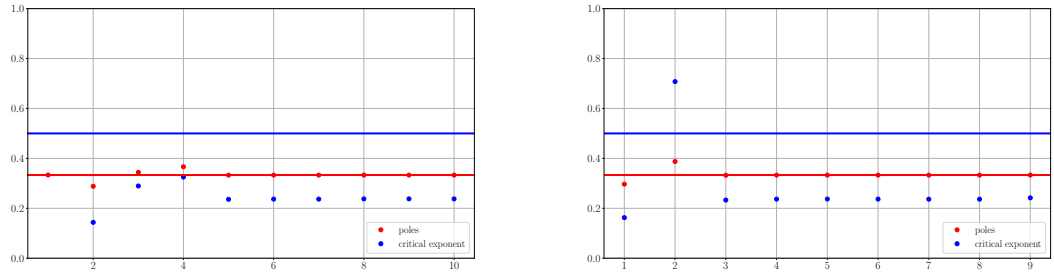

(a) $\Delta = +1$ (b) $\Delta = -1$

Figure 13: Comparison of the critical exponent and the position of poles with their expected values for the ratio $J = h$ for the families $\Delta = \pm 1$.

For this, both quantities once again converge nicely. However, the critical exponent does not approach 0.5 but instead lies around 0.24.

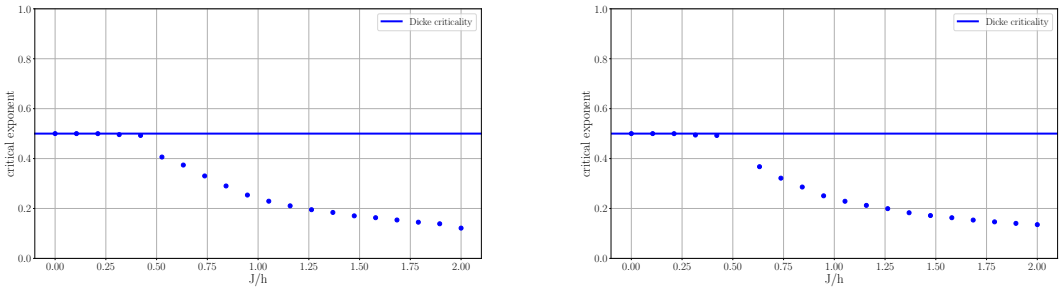

(a) [9,10] dlog-Padé (b) [10,9] dlog-Padé

Figure 14: Dependence of the critical exponent on the ratio of $\frac{J}{h}$ for two different dlog-Padés.

To examine this change in the critical exponent more closely, the critical exponent is calculated for different ratios of J/h at the expected transition point, as determined by Equation 43, using a single dlog-Padé. Figure 14 visualizes this. For both Dlog-Padés the critical exponent stays at $\frac{1}{2}$ till $\frac{J}{h} \approx 0.4$ and then starts to decrease. The reason for this cannot be explained, but it hints that the change in the order of the quantum phase transition occurs earlier than expected so far.

Another indicator for the type of quantum phase transition is the angle between the two ground-state energies at the critical point. A second-order transition should show a vanishing angle between the energies because it is continuous at the point of intersection, and the two energies have the same tangent at this point. On the other hand, the first derivative of a first-order phase transition is discontinuous, leading to a finite angle between the energies.

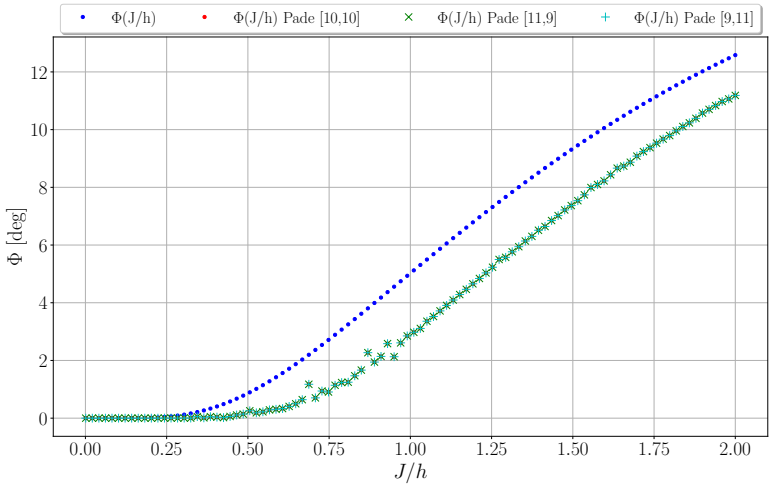

Figure 15: Angle between the ground-state energies of the strong and weak coupling limits depending on the ratio of $\frac{J}{h}$ using the bare series and Padé extrapolations.

Figure 15 shows this angle depending on the ratio of $\frac{J}{h}$. For the bare series the angle is zero till $J \approx 0.25h$ and for the Padé extrapolations until $J \approx 0.5h$. This can be explained with the better convergence of the Padé approximant. This result supports the hypothesis that the change in the order of the quantum phase transition takes place around $J \approx 0.5h$.

5. Results: antiferromagnetic Ising interactions

In this section the antiferromagnetic case is investigated. This means that J is positive in Equation 15. The aim of this is to compare the points of the quantum phase transition with the results obtained from a quantum Monte Carlo simulation (QMC). This simulation was performed by Anja Langheld [2]. In this case, only small values of h are considered because for antiferromagnetic interactions for larger h an intermediate phase occurs that can not be analyzed with the used perturbative approach.

5.1. Mapping to QMC Hamiltonian

The QMC was done for a fixed value of $J = 0.2$ and ω_c=1. Then, the point of the phase intersection was given as pair of g and h. So far the the ground-state energy and the magnetization were only calculated for $\frac{g^2}{\omega_c} = 2$. So it is necessary to generalize it to arbitrary ratios of $\frac{g^2}{\omega_c}$. This can be done for the fixed values of J and ω_c with the following transformation of the point of the intersection

$$g_{\mathrm{QMC}} = \frac{\sqrt{\frac{2}{0.2g}}}{2}. \tag{44}$$

Here g is the point of intersection obtained with the series for the Hamiltonian Equation 15. The square root is needed because the QMC used g and not g^2. Now, the data of the two methods can be compared by calculating the intersection between a Padé of the ground-state energy and a line with the slope $-J$.

5.2. Comparison to QMC

Figure 16 shows in magenta the points of the QMC and in blue the one obtained from the series expansion. The parameters J and h were fixed with the values from the QMC and g was calculated with Equation 44. The red and blue points match quantitatively so that the QMC could confirm the calculated series.

[2] Anja Langheld, Institut für Theoretische Physik I, Universität Erlangen-Nürnberg, anja.langheld@fau.de

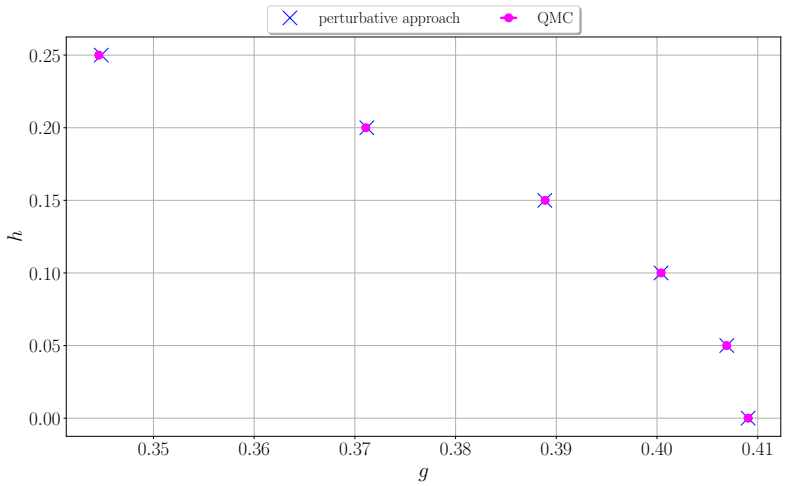

Figure 16: Comparison of the quantum phase transition points between QMC and the presented perturbative approach.

Now, the same procedure is done for values of h between 0 and 0.25 to get a continuous line through the points in Figure 16. For this, the intersection for different Padés of the ground-state energy is plotted to get an error for the calculation of the intersection. Figure 17 visualizes 200 ratios for $J = 0.2$ and h between 0 and 0.25. Most of these points lie on the expected line through the QMC point but some points are off. Latter probably deviate because the limited numerical precision of the calculation of the intersection and through the transformation Equation 44 applied to g that makes it very sensitive for deviations.

Overall, the QMC and the points, calculated in this thesis, match pretty good. So the comparison between these two could verify our perturbative approach to the quantum phase transition.

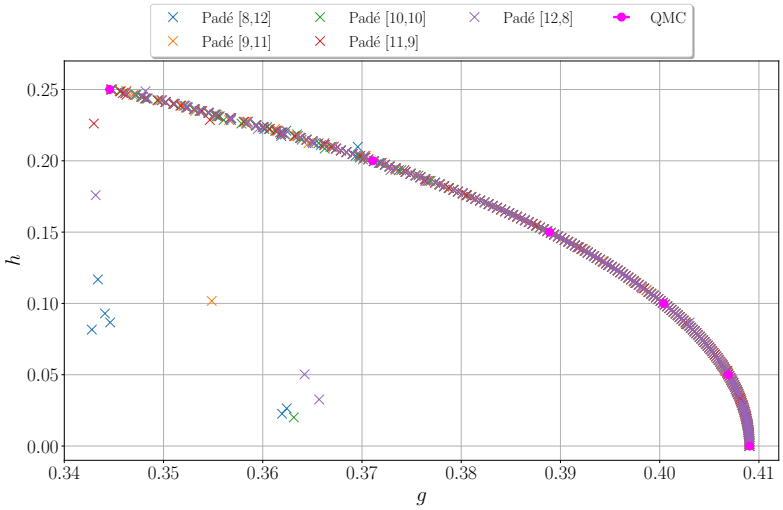

Figure 17: Point of intersection for values between $h = 0$ and $h = 0.25$.

6. Conclusions

The ground-state energy and magnetization of the Dicke-Ising chain were successfully calculated up to order 20 in the strong-coupling limit. The series exhibited the expected behavior for the limiting cases, namely, the Dicke chain and the quantized transverse-field Ising chain without a longitudinal field. The model has a second-order phase transition up to $J = 0.5h$ when approaching from the Dicke limit. This behavior is attributed to the critical exponent and the angle between the two energies at the phase transition. In the opposite limit, it becomes evident that the phase transition is of first order until $J = 2h$. This is because the energies do not intersect at the expected value anymore, and there is no longer a pole in the magnetization at the intersection point. In the region between $J = 0.5h$ and $J = 2h$, it is challenging to definitively classify the order of the phase transition and it is necessary investigate this region more closely. Remarkably, the pole of the magnetization aligns closely with the theoretically expected value, even for larger ratios of $\frac{J}{h}$ up to approximately $J = 1.5h$.

Furthermore, for the antiferromagnetic case, our findings match very well with data from quantum Monte Carlo simulations.

Overall, the results were pretty good and suggest the need for a more in-depth analysis of the change in the order of the quantum phase transition. Particularly for higher ratios of $\frac{J}{h}$, the reasons for the smaller critical exponents and the poles of the magnetization, which still match the expected values, are not explained. It would also be interesting to explore the behavior of the model on different lattices like the square lattice.

A. Appendix

A.1. Series of the magnetization

$$m(J,h) = \frac{1}{2} - \frac{2431h^{20}}{524288} - \frac{J^2}{8} - \frac{11J^4}{128} - \frac{51J^6}{512} - \frac{4607J^8}{32768} - \frac{28883J^{10}}{131072} - \frac{773119J^{12}}{2097152} - \frac{5409245J^{14}}{8388608} - \frac{2501886279J^{16}}{2147483648} - \frac{18531114459J^{18}}{8589934592} - \frac{559742586247J^{20}}{137438953472} - \frac{715h^{18}\left(4 - 144J + 2741J^2\right)}{524288} - \frac{h^{16}\left(82368 - 2635776J + 44914320J^2 - 541453824J^3 + 5178597667J^4\right)}{12582912} - \frac{h^{14}\left(228096 - 6386688J + 96106176J^2 - 1031498496J^3 + 8847974916J^4 - 64477710000J^5 + 414591467939J^6\right)}{28311552} - \frac{h^{12}\left(27869184 - 668860416J + 8734666752J^2 - 82245943296J^3 + 624977503488J^4 - 4071097128960J^5 + 23612294901312J^6\right)}{2717908992} - \frac{h^{12}\left(-125076649470464J^7 + 615846028873041J^8\right)}{2717908992} + h^{10}\left(-\frac{7}{512} + \frac{35J}{128} - \frac{6203J^2}{2048} + \frac{12577J^3}{512} - \frac{16027643J^4}{98304} + \frac{69414481J^5}{73728} - \frac{17342670893J^6}{3538944} + \frac{62361384529J^7}{2654208} - \frac{1071030868392403J^8}{10192158720} + \frac{16884325100457673J^9}{38220595200} - \frac{160886115102063685 57J^{10}}{9172942848000}\right) + h^8\left(-\frac{5}{256} + \frac{5J}{16} - \frac{2915J^2}{1024} + \frac{1245J^3}{64} - \frac{5495507J^4}{49152} + \frac{1742927J^5}{3072} - \frac{4614647243J^6}{1769472} + \frac{1216364429J^7}{110592} - \frac{218789530571827J^8}{5096079360} + \frac{248743646340119J^9}{1592524800} - \frac{244493481354059377 9J^{10}}{4586471424000} + \frac{246105392842194089 9J^{11}}{1433272320000} - \frac{346720051891984435334 3J^{12}}{660451885056000}\right) + h^6\left(-\frac{1}{32} + \frac{3J}{8} - \frac{345J^2}{128} + \frac{493J^3}{32} - \frac{152171J^4}{2048} + \frac{1445381J^5}{4608} - \frac{29019323J^6}{24576} + \frac{669435809J^7}{165888} - \frac{8088229085833J^8}{637009920} + \frac{3558332407829J^9}{95551488} - \frac{11791413637493089J^{10}}{114661785600} + \frac{386480162822500 97J^{11}}{143327232000} - \frac{465077839491002298107J^{12}}{687970713600000} + \frac{840935081561759522509 1J^{13}}{5159780352000000} - \frac{752250419105133303190 5227J^{14}}{1981355655168000000}\right) + h^4\left(-\frac{1}{16} + \frac{J}{2} - \frac{179J^2}{64} + \frac{93J^3}{8} - \frac{123307J^4}{3072} + \frac{138181J^5}{1152} - \frac{35762455J^6}{110592} + \frac{1234033J^7}{1536} - \frac{13270646647J^8}{7077888} + \frac{33098154791J^9}{7962624} - \frac{1013938089730 33J^{10}}{11466178560} + \frac{5208119355781J^{11}}{286654464} - \frac{2993946380775762 61J^{12}}{8255648563200} + \frac{364300356170244757J^{13}}{5159780352000} - \frac{266624746545936538907 27J^{14}}{198135565516800000} + \frac{233803791681705776425 31J^{15}}{92876046336000000} - \frac{264414568626117443096762827J^{16}}{570630428688384000000}\right) + h^2\left(-\frac{1}{4} + J - \frac{37J^2}{16} + \frac{19J^3}{4} - \frac{6677J^4}{768} + \frac{987J^5}{64} - \frac{719483J^6}{27648} + \frac{900059J^7}{20736} - \frac{124536593J^8}{1769472} + \frac{452272529J^9}{3981312} - \frac{103191412355J^{10}}{573308928} + \frac{13604744495J^{11}}{47775744} - \frac{183512318632519J^{12}}{412782428160} + \frac{14325289026103J^{13}}{20639121408} - \frac{8855770707711443J^{14}}{8255648563200} + \frac{1232795114126849J^{15}}{743008370688} - \frac{181577254010347786232 71J^{16}}{7132880358604800000} + \frac{116226438241330425580 01J^{17}}{2972033482752000000} - \frac{766172975242436048955 8641J^{18}}{1283918464548864000000}\right) \tag{45}$$

A.2. Series of the ground-state energy

$$E_0(J,h) = -\frac{1}{2} - \frac{J^2}{4} - \frac{3J^4}{64} - \frac{J^6}{32} - \frac{507J^8}{16384} - \frac{153J^{10}}{4096} - \frac{26641J^{12}}{524288} - \frac{1227J^{14}}{16384} - \frac{125526843J^{16}}{1073741824} - \frac{25577353J^{18}}{134217728} - \frac{11040019611J^{20}}{34359738368} - \frac{h^{12}J^6\left(381240 - 8285064J + 101738023J^2\right)}{248832} - \frac{h^{10}J^5\left(-6407424000 + 115686144000J - 1194527952000J^2 + 9008965134000J^3\right)}{8957952000} - \frac{h^{10}J^5\left(-54887151854400J^4 + 285137391997511J^5\right)}{8957952000} + h^8\left(-\frac{73J^4}{192} + \frac{65J^5}{12} - \frac{77531J^6}{1728} + \frac{177391J^7}{648} - \frac{2709839293J^8}{1990656} + \frac{2172752628813J^9}{37324800} - \frac{396779788709549J^{10}}{17915904000} + \frac{47716721889899J^{11}}{622080000} - \frac{21146959249337344909J^{12}}{85996339200000}\right) + h^6\left(\frac{J^3}{4} - \frac{41J^4}{16} + \frac{377J^5}{24} - \frac{20777J^6}{288} + \frac{1425553J^7}{5184} - \frac{569920823J^8}{622080} + \frac{2058392053J^9}{746496} - \frac{7624787805401J^{10}}{995328000} + \frac{357451628810473J^{11}}{17915904000} - \frac{21182684306496529 87J^{12}}{42998169600000} + \frac{2000658112866824313 83J^{13}}{1719926784000000} - \frac{3274187789493976518 2951J^{14}}{123834728448000000}\right) + h^4\left(-\frac{J^2}{4} + \frac{3J^3}{2} - \frac{185J^4}{32} + \frac{629J^5}{36} - \frac{158375J^6}{3456} + \frac{1127321J^7}{10368} - \frac{39878755J^8}{165888} + \frac{250414501J^9}{497664} - \frac{2894924916103J^{10}}{2866544640} + \frac{140360635571J^{11}}{71663616} - \frac{12710137866037117J^{12}}{3439853568000} + \frac{1405516178781996 41J^{13}}{20639121408000} - \frac{1219463783241869874631J^{14}}{99067782758400000} + \frac{6773546490873150798 53J^{15}}{30958682112000000} - \frac{3645933430153846591371071J^{16}}{95105071448064000000}\right) + h^2\left(-\frac{1}{2} + J - \frac{3J^2}{2} + \frac{9J^3}{4} - \frac{155J^4}{48} + \frac{75J^5}{16} - \frac{5777J^6}{864} + \frac{199763J^7}{20736} - \frac{2280025J^8}{165888} + \frac{9840743J^9}{497664} - \frac{1012622423J^{10}}{35831808} + \frac{2914963397J^{11}}{71663616} - \frac{23482377539J^{12}}{403107840} + \frac{108273272677J^{13}}{1289945088} - \frac{103587177790409J^{14}}{859963392000} + \frac{1291260032601 37J^{15}}{743008370688} - \frac{2784918990109892650 9J^{16}}{111451255603200000} + \frac{2011662481344661597 37J^{17}}{557256278016000000} - \frac{4172410848520876777337 3J^{18}}{80244904034304000000}\right) \quad (46)$$

Bibliography

[1] R. H. Dicke, "Coherence in spontaneous radiation processes," *Phys. Rev.*, vol. 93, pp. 99–110, 1954. DOI: 10.1103/PhysRev.93.99.

[2] Y. Zhang, L. Yu, J. Q Liang, G. Chen, S. Jia, and F. Nori, "Quantum phases in circuit QED with a superconducting qubit array," *Scientific Reports*, vol. 4, no. 1, 2014. DOI: 10.1038/srep04083.

[3] J. Rohn, M. Hörmann, C. Genes, and K. P. Schmidt, "Ising model in a light-induced quantized transverse field," *Phys. Rev. Res.*, vol. 2, p. 023 131, 2020. DOI: 10.1103/PhysRevResearch.2.023131.

[4] S. G. BRUSH, "History of the lenz-ising model," *Rev. Mod. Phys.*, vol. 39, pp. 883–893, 4 1967. DOI: 10.1103/RevModPhys.39.883.

[5] C. Gerry and P. Knight, *Introductory Quantum Optics*. Cambridge University Press, 2004. DOI: 10.1017/CBO9780511791239.

[6] F. Utermohlen, "Mean field theory solution of the ising model," 2018.

[7] E. Schrödinger, "Quantisierung als eigenwertproblem," *Annalen der Physik*, vol. 385, no. 13, pp. 437–490, 1926. DOI: https://doi.org/10.1002/andp.19263851302.

[8] P. Löwdin, "Studies in Perturbation Theory. IV. Solution of Eigenvalue Problem by Projection Operator Formalism," *Journal of Mathematical Physics*, vol. 3, no. 5, pp. 969–982, 1962. DOI: 10.1063/1.1724312.

[9] L. G. Marland, "Series expansions for the zero-temperature transverse ising model," *Journal of Physics A: Mathematical and General*, vol. 14, no. 8, p. 2047, 1981. DOI: 10.1088/0305-4470/14/8/027.

[10] R. P. Feynman, "Forces in molecules," *Phys. Rev.*, vol. 56, pp. 340–343, 1939. DOI: 10.1103/PhysRev.56.340.

[11] G. A. Baker Jr and J. L. Gammel, "The padé approximant," *Journal of Mathematical Analysis and Applications*, vol. 2, no. 1, pp. 21–30, 1961.

[12] A. Schellenberger, "Spectral properties of the one- and two-quasi-particle channel in the polarized phase of the kitaev model with external magnetic field," *Institute for Theoretical Physics I, Friedrich-Alexander-Universität Erlangen-Nürnberg*, 2021.

[13] P. Adelhardt, "Quantum criticality of long-range generalized quantum spin systems," *Institute for Theoretical Physics I, Friedrich-Alexander-Universität Erlangen-Nürnberg*, 2020.

[14] P. Pfeuty, "The one-dimensional ising model with a transverse field," *Annals of Physics*, vol. 57, no. 1, pp. 79–90, 1970. DOI: https://doi.org/10.1016/0003-4916(70)90270-8.

Acknowledgments

I would like to express my gratitude to Prof. Dr. Kai Phillip Schmidt for providing me with the incredible opportunity to work on this thesis. Additionally, I extend my appreciation to my supervisors, Anja Langheld and Dr. Max Hörmann, for their prompt and invaluable assistance whenever I faced challenges. My time in Theory 1 passed swiftly, thanks to the warm and supportive atmosphere within the whole group.

Eigenständigkeitserklärung

Hiermit versichere ich, dass ich die vorliegende Bachelorarbeit selbständig verfasst und keine anderen als die angegebenen Quellen und Hilfsmittel verwendet habe. Diese Arbeit hat in gleicher oder ähnlicher Form noch keiner Prüfungsbehörde vorgelegen.

Erlangen, den 4.10.2023

Jonas Leibig